Longitudinal spin relaxation time of donor-bound electrons in a CdTe quantum well

G. Garcia-Arellano, C. Testelin, Frédéric Bernardot, Maria Chamarro, Karczewski G.

Longitudinal spin relaxation time of donor-bound electrons in a CdTe quantum well

G. Garcia-Arellano,[1] F. Bernardot,[1] G. Karczewski,[2] C. Testelin,[1] and M. Chamarro[1]
[1]*Sorbonne Université, CNRS, Institut des NanoSciences de Paris, 4 place Jussieu, F-75005 Paris, France*
[2]*Institute of Physics, Polish Academy of Sciences, Al. Lotników 32/46, PL-02668 Warsaw, Poland*

(Received 26 June 2020; revised 7 September 2020; accepted 14 October 2020; published 29 October 2020)

We study the magnetic-field dependence of the longitudinal spin relaxation time T_1 of donor-bound electrons placed in the middle of an 8-nm CdTe quantum well with different doping concentrations in the range from 1×10^9 to 2.9×10^{11} cm^{-2} and at low temperature. We use an extended photoinduced Faraday rotation technique, which expands the usual domain of the measured decays from tens of ns to μs. As in high-purity bulk semiconductors, a maximum relaxation time of around $T_1 \sim 10$ μs is observed for a residually doped sample at low magnetic field of $B = 0.08$ T. For higher doping concentrations, the magnetic-field dependence of T_1 shows a nonmonotonic behavior: first a rapid increase, followed by a plateau or a decrease of T_1. The fast increase of T_1 at low magnetic fields is explained by the inhibition of the mechanisms identified at zero field—hyperfine and anisotropic exchange interactions—while the behavior at high magnetic field can be succesfully explained by a mechanism proposed by Lyubinskiy and associated to electron hops [I. S. Lyubinskiy, JETP Lett. **88**, 814 (2008)]. A good agreement between experiment and theory is found for samples below the metal-insulator transition, when Dresselhaus terms of spin-orbit coupling are considered to be the dominant ones in the Hamiltonian describing the system.

DOI: 10.1103/PhysRevB.102.165314

I. INTRODUCTION

In the last decade, electron-spin dynamics in semiconductors has attracted much attention due to the possibility of using the electron spin as a qubit. Shallow impurities in direct-band-gap semiconductor materials are especially interesting, in this sense, due to their optical addressability, strong spin-photon coupling, and long spin relaxation times [1–4].

An ensemble of localized electrons subject to a magnetic field is characterized by two relaxation times [5]: the longitudinal spin relaxation time T_1, which is related to the relaxation of the spin component parallel to the field, and the transverse relaxation time T_2^*, which describes the dephasing of the spin ensemble due to the inhomogeneous broadening. When the main source of inhomogeneities for electrons bound to donors is related to the Landé factor inhomogeneities, the T_2^* extrapolated to zero magnetic field leads to the spin dephasing time of a single electron T_2, which is equal to T_1 at zero magnetic field.

In the absence of magnetic field, T_1 has been determined in different direct-band-gap semiconductors: GaAs [6–8], ZnSe [9,10], CdTe [11–13], ZnO [14], GaN [15,16], InSb [17], and InAs [18]. Recently, the influence of doping concentration on the spin relaxation time T_1 in the insulating regime and at low temperature was revisited in GaAs [7,8] and CdTe [11,12], reporting a nonmonotonic behavior exhibiting a maximum value near the metal-insulator transition (MIT). The origin of the observed maximum was explained by the interplay between the hyperfine interaction and the anisotropic exchange interaction. The first one dominates at low donor concentrations and the latter one becomes more important for concentrations near the MIT [7,12].

At low doping concentrations and liquid-helium temperature, donors do not interact with each other and localize a single electron in their vicinity. In this situation, neutral donors in semiconductors are very similar to doped quantum dots. It has been shown that, as in quantum dots, the spin relaxation time of a donor-bound electron is limited by its interaction with the nuclear spins [19,20].

For doping concentrations near the MIT, different donor sites interact. In semiconductors with a lack of inversion symmetry, the exchange interaction plus the spin-orbit coupling lead to an anisotropic term of the exchange Hamiltonian that is responsible for the electron-spin relaxation at zero magnetic field [21,22].

Longitudinal spin relaxation time T_1 as a function of magnetic field has been less explored. Up to now, most of the studies are centered on low-temperature and very pure samples or samples with very low doping concentrations in bulk GaAs, CdTe, and InP [3,23,24]. Recently, a study has also been performed in bulk wurzite and high-purity ZnO [25]. Very few studies, and only in bulk GaAs, have explored the influence of doping concentration in the insulating regime and at low temperature [26–28].

Up to now, there is no unified model that explains the magnetic-field dependence of T_1 for different concentrations. Only the magnetic-field behavior of T_1 at very low concentrations is mostly understood [24].

For GaAs and InP samples with very low doping concentrations, T_1 follows, at low magnetic fields, a B^2 dependence with a proportionality constant dependent on donor concentration [24]. This increase of T_1 with magnetic field, when Zeeman splitting is negligible as compared to thermal energy, is associated with the screening of the nuclear field

TABLE I. Doping concentration, electron Landé factor $g_e^{\perp}$, spin relaxation time at zero magnetic field $T_1(0)$, and excitation energy for the different samples used in this work.

Sample	Doping concentration (donors/cm^2)	Electron Landé factor $g_e^{\perp}$	Spin relaxation time $T_1(0)$ (ns)	Excitation energy (eV)
I	1×10^9	1.39	4.5	1.622
II	9.7×10^{10}	1.44	13.3	1.611
III	1.6×10^{11}	1.45	12.5	1.615
IV	2.9×10^{11}	1.40	4.1	1.617

fluctuations. At high magnetic fields, samples with residual concentrations show a $B^{-\nu}$ dependence of T_1 with $3 < \nu < 4$. For CdTe and GaAs samples, a direct spin-phonon interaction was identified at the origin of this behavior. Moreover, for GaAs, a relaxation between donor-bound electron ground state mediated by spin-orbit and electron-phonon coupling like in III–V quantum dots is significant and at the origin of a $B^{-\nu}$ dependence ($4 < \nu < 5$) [29].

In this work, we center our study on a system that emerged some years ago as a good prototype for spintronic applications: donor-bound electrons immersed in the middle of a quantum well (QW), since experimental studies revealed that the additional localization of the electron bound to donor wave function by a QW leads to an enhancement of the spin relaxation time [30]. Besides, it presents a higher degree of optical orientation of the electron spins than three-dimensional crystals, and it is a very homogeneous system with a reduced spin-nuclear environment [31–34].

We use an extended photoinduced Faraday rotation technique (PFR) [27] to measure the longitudinal spin relaxation time T_1 of donor-bound electrons immersed in the middle of a 8-nm CdTe QW in a doping range spanning from 1×10^9 to 2.9×10^{11} donors. cm^{-2} and at low temperature. We have explored the magnetic-field dependence of T_1 in CdTe because, while having the same crystal structure as GaAs, this semiconductor has different parameters that determine the spin relaxation time, such as the strength of the spin-orbit interaction, the binding energy, and the electron Landé factor [12]. Furthermore, II–VI materials are potentially attractive to enhance spin coherence times thanks to the isotopic purification [32].

We have found that, at any doping concentration, the application of a weak longitudinal magnetic field leads to a fast increase of the spin relaxation time, while for higher magnetic fields, T_1 remains constant or slightly decreases. As it was found in bulk high-purity semiconductors [24], the sample with a residual doping concentration shows the longest spin relaxation time of the order of $T_1 \sim 10\ \mu s$. For higher doping concentrations, a nonmonotonic behavior of T_1 is observed: first a rapid increase, followed by a constant or decreasing T_1. We have explained the first fast increase, for all the samples, by the suppression of the efficient relaxation mechanisms at zero magnetic field, namely hyperfine and anisotropic exchange interactions. For higher magnetic fields and donor concentrations below the MIT, the almost constant value or decrease of T_1 can be suceessfully explained by a mechanism due to electrons hops, assuming that the Dresselhaus spin-orbit term is the dominant one in a symmetric QW [35].

II. SAMPLES AND EXPERIMENTAL SETUP

The studied samples consist of a CdTe/CdMgTe heterostructure grown by molecular-beam epitaxy on a (100)-oriented GaAs substrate and containing an 8-nm CdTe QW. The samples were doped with iodine atoms placed in the midplane of the QW, each with a different doping concentration: (I) 1×10^9 cm^{-2}, (II) 9.7×10^{10} cm^{-2}, (III) 1.6×10^{11} cm^{-2}, and (IV) 2.9×10^{11} cm^{-2}. The spin relaxation time $T_2(0) = T_1(0)$ and the transverse electron Landé factor $g_e^{\perp}$ have been determined in a previous study for each of the samples (see Fig. 5 of Ref. [12]). Table I gathers the characteristics of the studied samples.

We have chemically suppressed the GaAs substrate to measure the PFR signals by transmission and study in this way the longitudinal spin dynamics of resident electrons. In particular, we used an extended pump-probe technique [27]. The light source is a Ti:sapphire laser beam with a 2-ps pulse duration and a 76-MHz repetition rate (repetition period $T_R = 13.1$ ns), which is split into pump and probe beams.

In the pump path, an electronic gate is created by an electro-optic modulator (EOM), which selects an ensemble of N pulses, each of them separated by T_R, with an arbitrary long delay between two consecutive gates. An acousto-optic modulator (AOM) is used in the probe path for the same purpose. The AOM and the EOM are synchronized and the time width of each gate can be chosen with a minimum value of 50 ns (three lasers pulses). The time delay between the gates produced by the EOM and the AOM is controlled electronically with a maximum delay of 3μs. The polarization of the pump beam was modulated between σ_+ and σ_- by a photoelastic modulator (PEM) working at 50 kHz to avoid any nuclear polarization. The half period (10 μs) of the PEM modulation fixes the upper limit of our measurement time scale. The probe beam is linearly polarized, and its intensity is modulated with a chopper at 500 Hz. The rotation angle of the probe beam polarization is analyzed, after transmission through the sample, by an optical bridge. A double lock-in amplifier is used in order to improve the signal-to-noise ratio. The sample was placed in a liquid-helium cryostat and a magnetic field was applied parallel to the growth direction (Faraday geometry) using a superconducting split-coil magnet.

III. EXPERIMENTAL RESULTS

In Fig. 1, we present the PFR signal measured as a function of pump-probe delay for samples II–IV, and for different magnetic fields at 2 K. The common pump and probe energy is always tuned to the D^0X transition (see Table I). By tuning

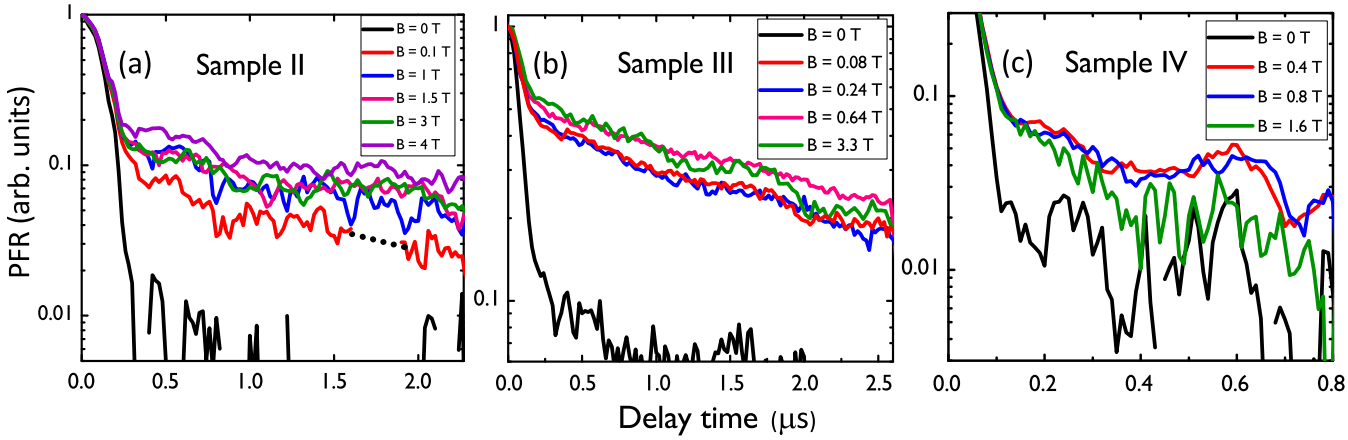

FIG. 1. PFR signal obtained for different longitudinal magnetic fields at 2 K, by tuning the laser to D^0X transition of samples II, III, IV. The temporal widths of the pump and probe gates denoted as w_{pump}, w_{probe} are respectively: (a) $w_{pump} = w_{probe} = 150$ ns, window $= 3\,\mu$s; (b) $w_{pump} = w_{probe} = 100$ ns, window $= 3\,\mu$s; (c) $w_{pump} = w_{probe} = 60$ ns, window $= 1\,\mu$s. The response of the experimental set-up at zero magnetic field is represented by a black solid line in each figure.

pump and probe energies at the D^0X transition, we create mainly donor-bound excitons, since the bandwidth of the used mode-locked Ti:sapphire laser is less than 1 meV. Under these excitation conditions, in a previous work using Voigt configuration [12], we observed an oscillatory signal with a decay time larger than the lifetime of D^0X. This long-lasting signal was associated to the signature of the spin polarization of electron bound to donors D^0. In the following we will center our study in this long decay signal also observed at zero magnetic field.

The focus spot area is $(90\,\mu\text{m})^2$ and the energy fluence of the pump pulses is $0.5\,\mu\text{J cm}^{-2}$. The widths of the optical trains and the needed temporal window chosen for each sample are indicated in the corresponding figure captions. In order to keep a detectable level of signal, the widths of the gates have been increased only when a longer temporal window was needed. We see that the application of a longitudinal magnetic field slows down the spin dynamics in the studied samples. The fast decay observed at the first hundreds of nanoseconds corresponds to the overlapping of the pump and probe trains near $t = 0$. Note that at $B = 0$ the measured longitudinal spin relaxation time T_1 should be equal to the spin dephasing time T_2, obtained by extrapolation in Ref. [12]. Since T_2 has been found to be less than 20 ns, the signal obtained at $B = 0$ (black curves) represents the response of the experimental setup.

For samples II and III, a slow component in the microsecond range appears quickly when the magnetic field is slightly increased. For sample IV, with a donor concentration close to the MIT, the spin relaxation decay is faster than for samples II and III. For all the samples, an exponential decay of the signal is observed.

Figure 2 summarizes the measured T_1 at 2 K as a function of the Zeeman splitting for the four different samples described in Table I. The absolute values of the electron Landé factors taken to calculate the Zeeman splitting are also listed in Table I. We have used the value of $g_e^{\perp}$ since $g_e^{\perp} \approx g_e^{\parallel}$ for localized electrons in a CdTe/CdMgTe QW [36]. The inset of Fig. 2 shows the PFR decay obtained in sample I, with the lowest doping concentration, at $B = 80$ mT and $T = 2$ K. As it has been observed in bulk GaAs, CdTe, and InP [24], residually doped samples show very long spin relaxation times. The estimated time of $T_1 \sim 10\,\mu$s for sample I at the Zeeman splitting energy of $6.5\,\mu$eV reaches the maximum relaxation time that can be measured with our experimental setup. In Ref. [24], a crossover point between the high and low magnetic regimes has been observed for high-purity bulk GaAs and InP; for the CdTe samples, with a doping concentration of $1 \times 10^{14}\,\text{cm}^{-3}$ (which corresponds approximately to a surface concentration of $2 \times 10^9\,\text{cm}^{-2}$), a decrease of T_1 is only observed for Zeeman splittings in the range of 0.1–0.6 meV. The measured time for sample I (with a comparable doping concentration) at lower Zeeman splitting may indicate that a crossover point also exists for CdTe. We underline that the

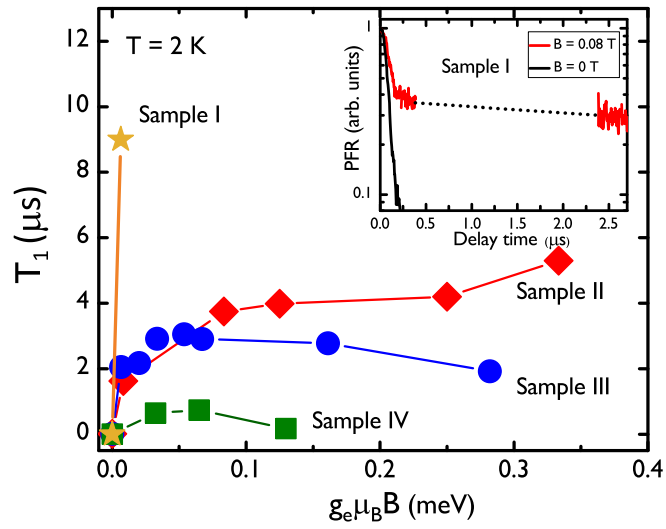

FIG. 2. Longitudinal spin relaxation time T_1 as a function of the Zeeman splitting for samples I–IV. Inset: PFR signal obtained with sample I, for $B = 80$ mT and $T = 2$ K. The laser was tuned at 1.622 eV. The response of the experimental setup at zero magnetic field is represented by a black solid line.

experimentally observed T_1 in sample I is larger than the one obtained in Ref. [28] of $T_1 \approx 2\,\mu$s, for a bulk GaAs sample with a doping concentration of $5.5 \times 10^{14}\,\mathrm{cm}^{-3}$ and at the same Zeeman splitting.

For the sample with an intermediate doping concentration, sample II, we observed a continuous increase of the spin relaxation time with the applied magnetic field, followed by a plateau which shows a slight tendency to increase at the higher Zeeman splittings. For samples III and IV, the same qualitative behavior as a function of magnetic field is observed: first an increase, that is faster than in sample II, and then a plateau or a maximum, which is obtained at lower Zeeman splitting than in sample II. At higher magnetic fields, a slight decrease of T_1 is observed for samples III and IV. In general, as the concentration is increased from sample II to sample IV, the maximum T_1 value decreases.

There are no available experimental results in the literature concerning the behavior as a function of magnetic field of T_1 in CdTe samples with donor concentrations larger than residual ones. Results on bulk GaAs show that $T_1(B)$ depends strongly on concentration [23,26,28]. Up to now, there is no unified model that explains the magnetic-field dependence of T_1 at different doping concentrations, either in bulk or in QWs. In order to explain the observed magnetic-field dependence of T_1 in a QW, we will consider that, at low magnetic field, the two main mechanisms responsible for the spin relaxation at zero magnetic field, the hyperfine interaction and the anisotropic exchange interaction, are inhibited by the application of a magnetic field, while at higher magnetic field, we will use the model proposed by Lyubinskiy for QWs [35] associated to electron hops, described here below.

IV. MAGNETIC-FIELD DEPENDENCE OF T_1: THEORETICAL DESCRIPTION

At zero magnetic field, in the low-density regime, the dominant mechanism that contributes to the spin relaxation time of donor-bound electrons in a CdTe QW is the hyperfine interaction, which can be expressed in terms of a random effective nuclear field applied to the localized electron spin [19,37]. For higher impurity concentrations (below the MIT), the dominant mechanism is the anisotropic exchange interaction induced by the spin-orbit interaction [7,12,21]. Both dynamics are driven by a correlation time τ_c. When a weak magnetic field is applied, the relaxation slows down and, in the motional-narrowing regime, the relaxation rate is reduced and can be written as [38]

$$\frac{1}{\tau_s^c} = \frac{1}{\tau_s(0)} \frac{1}{1 + (\Omega_0 \tau_c)^2}, \tag{1}$$

with $\hbar\Omega_0 = g\mu_B B$ the Zeeman splitting and $\tau_s(0) = T_1(0)$ the zero-field relaxation time, controlled by hyperfine interaction or anisotropic exchange coupling.

The spin relaxation time given by Eq. (1) is represented by a blue dotted line in Fig. 4. We underline that the observed increase of T_1 in all the samples at weak magnetic fields can be explained by the inhibition of the mechanisms driven by the correlation time: hyperfine interaction and anisotropic exchange interaction. The values found for the correlation time τ_c for each of the samples is reported in Table II. As expected, this value decreases as the doping concentration increases, and it is close to the one calculated from the exchange energy of a pair of donor-bound electrons immersed in the middle of an infinite QW [12].

TABLE II. Correlation time τ_c and time constant τ_0 found from the fit of the experimental data of the longitudinal spin relaxation time with Eq. (13) for samples II–IV (see Fig. 4).

Sample	τ_c (ps)	τ_0 (ps)
II	400	0.5
III	400	0.35
IV	200	0.06

For isolated spins, as we have already described in the Introduction, the dominant mechanism that contributes to the spin relaxation time at high magnetic fields is mainly the admixture mechanism, caused by the spin-orbit coupling and electron-phonon interaction [39]. A power-law dependence of $T_1 \propto B^{-\nu}$ is expected, with $4 < \nu < 5$, as observed with impurities [24] or quantum dots [29]. For isolated donors in bulk direct-band-gap semiconductors as GaAs, CdTe, and InP, direct spin-phonon processes may have a comparable contribution to the spin relaxation time, reducing the exponent value to $3 < \nu < 4$ [24]. Applying a magnetic field, one then expects a decrease of the relaxation rate, followed by an increase at high field.

For impurity concentrations larger than residual ones and in the insulating regime, another mechanism induced by the spin-orbit interaction has been proposed to explain the spin relaxation time of localized electrons in two-dimensional (2D) semiconductor QWs in presence of an applied longitudinal magnetic field [35]. This mechanism involves phonon-assisted electron hops from one donor to another. This model is based on the idea that the ensemble of localized electrons is grouped in small clusters, inside of which an electron is coupled with the rest of the donor-bound electrons by isotropic exchange, but it also may visit other clusters by hopping diffusion. In the absence of magnetic field, it has been shown that for localized electrons, this mechanism is less efficient than isotropic exchange [38]. The hops are accompanied by absorption or emission of acoustic phonons. While the electron hops from donor to donor, its spin experiences random rotations. The spin orientation vanishes after a large number of hops. So far this model could not be tested due to the lack of experimental results in QWs.

In the following, we will describe the main elements of this model. The hopping times of an electron between two donor sites depend exponentially on the distance r between the donors and on the energy difference E, between the energy levels in the impurity band. They are given by

$$\tau_{h1} = \tau_0 e^{2r/a_B}, \tag{2a}$$

$$\tau_{h2} = \tau_0 e^{2r/a_B + E/k_B T}, \tag{2b}$$

for phonon emission and absorption respectively, with a_B the Bohr radius of a donor-bound electron in a QW, k_B the Boltzman constant, and T the temperature. The derivation of the spin relaxation time due to this mechanism is given in

Ref. [35]. The Hamiltonian of the system is

$$H = \frac{\boldsymbol{p}^2}{2m} + U(\boldsymbol{r}) + \frac{\hbar}{2}\boldsymbol{\Omega}_0 \cdot \boldsymbol{\sigma} + \frac{\hbar}{2mL_s}\boldsymbol{\sigma}\,\hat{\alpha}\,\boldsymbol{p}, \tag{3}$$

where $\boldsymbol{r}$ is the position vector on an electron that hops between two donor sites at the positions $\boldsymbol{r}_1$ and $\boldsymbol{r}_2$, $U(\boldsymbol{r})$ is the impurity potential, L_s the length characterizing the strength of the spin-orbit coupling, m is the effective electron mass, $\hat{\alpha}$ is a dimensionless tensor with components of the order of unity, and $\boldsymbol{\sigma}$ is the vector of Pauli matrices. The last term in Eq. (3) is a combination of the Bychkov-Rashba spin-orbit coupling [40] and Dresselhaus spin-orbit coupling [41] averaged over the electron motion in the direction perpendicular to the QW. For a symmetric QW, the Dresselhaus term dominates [22], then the $\hat{\alpha}$ tensor and L_s are given by

$$\hat{\alpha} = \begin{pmatrix} 1 & 0 \\ 0 & -1 \end{pmatrix}, \tag{4}$$

$$\frac{1}{L_s} = \frac{\alpha\hbar\langle k_z^2\rangle}{\sqrt{2mE_g}}, \tag{5}$$

where E_g is the energy band gap, α is the dimensionless spin-orbit constant, and $\langle k_z^2\rangle$ is the quadratic average of the wave-vector component along z. After a unitary transformation, the Hamiltonian in Eq. (3) is transformed to [35]

$$\bar{H} = \frac{\boldsymbol{p}^2}{2m} + U(\boldsymbol{r}) + \frac{\hbar}{2}\boldsymbol{\Omega}_0 \cdot \boldsymbol{\sigma} + \frac{\hbar}{2}\left[\boldsymbol{\Omega}_0 \times \hat{\alpha}\,\frac{\boldsymbol{r}}{L_s}\right] \cdot \boldsymbol{\sigma}, \tag{6}$$

from which the spin dynamics equation is derived:

$$\frac{\partial \boldsymbol{S}}{\partial t} = [\boldsymbol{\Omega}_0 + \Delta\boldsymbol{\Omega}(\mathrm{t})] \times \boldsymbol{S}, \tag{7}$$

with $\Delta\boldsymbol{\Omega}(\mathrm{t}) = \boldsymbol{\Omega}_0 \times \hat{\alpha}\,\boldsymbol{r}(t)/L_s$, whose module $\Delta\Omega$ corresponds to the spin precession frequency in a random magnetic field. Then, the spin relaxation rate on a pair of impurities is derived from the random field correlator $\kappa(t) = \langle\Delta\boldsymbol{\Omega}(\mathrm{t}), \Delta\boldsymbol{\Omega}(0)\rangle$, giving [35]

$$\frac{1}{\tau_s^h}(\boldsymbol{r}, E) = \frac{\Delta\Omega^2}{4\cosh^2\left(\frac{E}{2T}\right)}\frac{\tau_h}{1 + (\Omega_0\tau_h)^2} \tag{8}$$

with $1/\tau_h = 1/\tau_{h1} + 1/\tau_{h2}$. Assuming a simple distribution law for the distance E between the energy levels and for the distance r between the donors, Lyubinskiy expressed the average spin relaxation rate as [35]

$$\frac{1}{\tau_s^{\mathrm{hop}}(B)} = \frac{1}{W}\frac{1}{L_d^2}\int \frac{1}{\tau_s^h(\boldsymbol{r}, E)} d\boldsymbol{r}dE, \tag{9}$$

with W the width of the impurity band defined as $W = e^2/4\pi\varepsilon_0\varepsilon L_d$, ε the dielectric constant, and $L_d = n_d^{-1/2}$ the average distance between donors. Making some approximations when calculating the integral in Eq. (9), the spin relaxation rate τ_s^L due to electron hops is written in Ref. [35] as [42]

$$\frac{1}{\tau_s^L} = \frac{\pi^2}{32}\frac{k_BT}{W}\left(\frac{a_B}{L_s}\frac{a_B}{L_d}\right)^2\frac{1}{\tau_0}\left[\Omega_0\tau_0 \ln^3\left(\frac{1}{\Omega_0\tau_0}\right)\right] \tag{10a}$$

for $\Omega_0\tau_0 < 1$, and

$$\frac{1}{\tau_s^L} = \frac{3\pi\ln 2}{4}\frac{k_BT}{W}\left(\frac{a_B}{L_s}\frac{a_B}{L_d}\right)^2\frac{1}{\tau_0} \tag{10b}$$

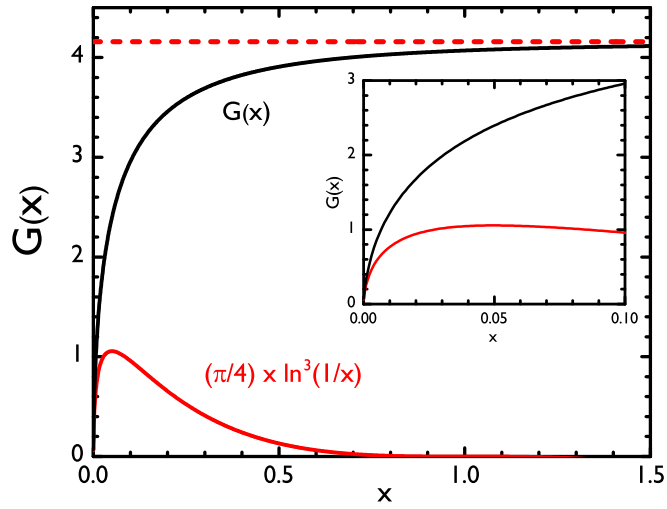

FIG. 3. Black solid line: plot of the function $G(x)$ in the range $0 < x < 1.5$ [see Eq. (12)]. The red solid line represents the function proposed by Lyubinsky in Ref. [35] as an approximation valid for small values of x. The red dashed line represents the asymptotic value at large x, conducting to Eq. (10b). Inset: same curves, in the range $0 < x < 0.1$.

for $\Omega_0\tau_0 > 1$.

In this work, we have calculated the integral appearing in Eq. (9) without approximations, obtaining an exact expression for the spin relaxation time, which is valid for all $\Omega_0\tau_0$ values:

$$\frac{1}{\tau_s^{\mathrm{hop}}} = \frac{\pi}{8}\frac{k_BT}{W}\left(\frac{a_B}{L_s}\frac{a_B}{L_d}\right)^2\frac{1}{\tau_0}G(\Omega_0\tau_0), \tag{11}$$

with $G(x)$ a function that can be calculated numerically:

$$G(x) = \frac{1}{2}\int_0^1 dz\left(\ln\frac{1}{z}\right)^3 \ln\left(\frac{z^2 + x^2}{z^2 + \frac{x^2}{4}}\right). \tag{12}$$

In Fig. 3, the black solid line represents the function $G(x)$. The red line represents the function $(\pi/4)x\,\ln^3(1/x)$ in Eq. (10a) proposed by Lyubinskiy [35] as an approximation of the function $G(x)$ for small values of x. The inset of Fig. 3 shows that this approximation is good only for very small values of x. The red dashed line represents the asymptotic value 6ln2 at large x, conducting to Eq. (10b).

Finally, the magnetic-field dependence of the longitudinal spin relaxation time of donor-bound electrons, T_1, at low temperature in the insulating regime can be written when the two already described contributions are taken into account: (i) the inhibition of the hyperfine and anisotropic exchange interactions [Eq. (1)], and (ii) the hopping mechanism [Eq. (11)], as follows:

$$\frac{1}{T_1(B)} = \frac{1}{\tau_s^c} + \frac{1}{\tau_s^{\mathrm{hop}}} \tag{13}$$

on the full magnetic field range. In Fig. 4, we have fitted the experimental data (full symbols) according to Eq. (13), using only two fitting parameters: the correlation time τ_c, at low magnetic fields, and the time constant τ_0, at high magnetic fields. We emphasize that all the other parameters have been deduced from previous zero-field studies ($a_B = 4.54$ nm,

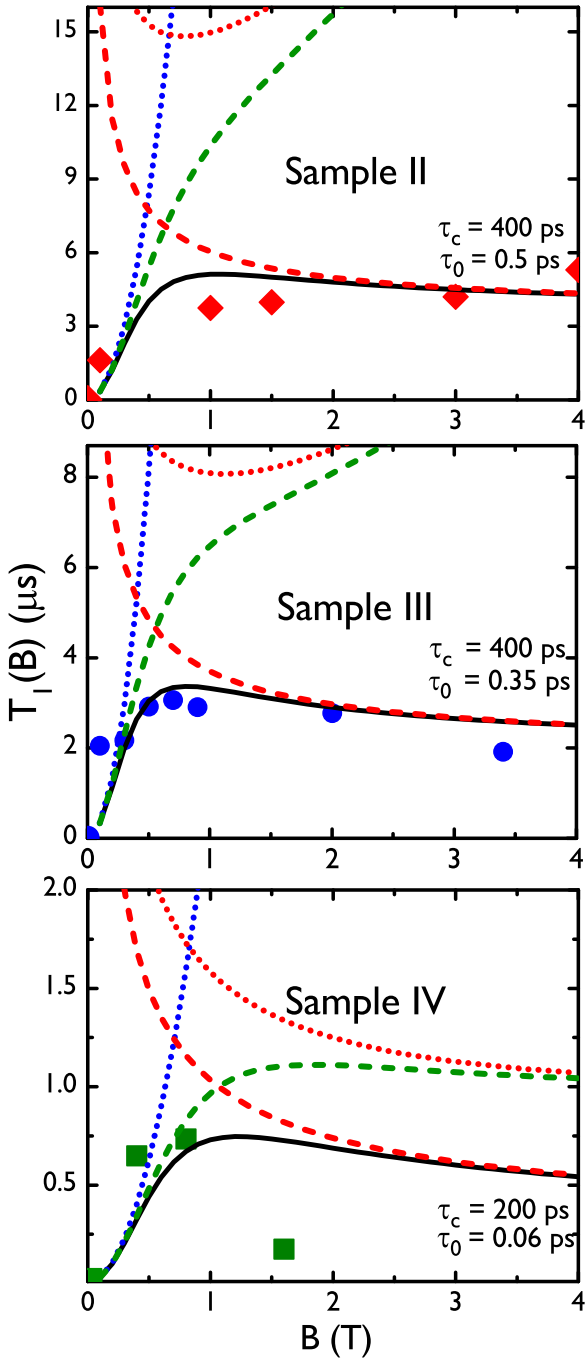

FIG. 4. Measured longitudinal spin relaxation times of electrons bound to donors in samples II–IV (full diamonds, disks, and squares, respectively). The two considered relaxation mechanisms are represented: (blue dotted line) inhibition of the mechanism driven by the correlation time τ_s^c [see Eq. (1)] and (red dashed line) electron hopping [see Eq. (11)]. The red dotted line represents the spin relaxation time due to the electron hopping according to Eq. (10a). The black solid line shows the spin relaxation time as a function of the magnetic field according to Eqs. (13) and (11). The dashed green line represents the spin relaxation time resulting from Eqs. (13) and (10a) proposed by Lyubinskiy.

$L_s = 446$ nm), from direct relation with the donor concentration (L_d, W) or experimental measurements [$g_e^{\perp}$, $\tau_s(0), T$]. The different relaxation times are shown in Fig. 4: the blue dotted line is related to the relaxation time τ_s^c governed by hyperfine and/or anisotropic exchange interaction [Eq. (1)], and the red dashed line represents the spin relaxation time τ_s^{hop} due to electron hops given by Eq. (11). The black solid line represents the theoretical magnetic-field dependence on the full magnetic field range of T_1, according to Eq. (13). The values of the fitting parameters τ_c and τ_0 are reported in Table II. We remark that the observed plateau or decrease of T_1 at high magnetic fields in samples II and III can be successfully explained by the hopping mechanism, and the agreement between theory and experience is slightly less good for high magnetic field in sample IV. For samples II and III, the agreement in amplitude and field dependence between experimental data and theoretical results is remarkable since the theoretical expressions are very sensitive to the material input parameters due to power laws (a_B^4, L_s^2, L_d^2).

For comparison, we have also drawn in Fig. 4 (red dotted line) the magnetic-field dependence of T_1 by using the approximate function proposed by Lyubinskiy [Eq. (10a)]. We remark that a better agreement with the experiment is found with the exact function $G(x)$ and Eq. (13), for all the samples. However, for sample IV, the model does not reproduce the high-field behavior of T_1. The donor concentration of this sample is very close to the MIT, with a large impurity band width and a small distance L_d. One certainly reaches the limit of this model, with parameters difficult to define, like the impurity-band width W, or space dependences more complex than the one used in our calculation, like $\tau_h(r)$. Moreover, other relaxation mechanisms, not considered in this work, are possible. Sample IV being close to the MIT, a small fraction of the electrons might be delocalized, inducing extra interaction and relaxation of one-site electron spin. Besides, by increasing the number of doping layers, one raises the density of off-centered donors in the QW, breaking the symmetry in the electron environment and inducing a Rashba coupling. Taking into account these additional mechanisms is beyond the scope of this work.

V. CONCLUSION

We have measured longitudinal spin relaxation times T_1 in the μs range for donor-bound electrons placed in the middle of an 8-nm CdTe QW, by means of an extended PFR technique. The magnetic-field dependence of T_1 was measured for different doping concentrations in the insulating regime and at low temperature. For any doping concentration, we have observed a fast increase of the spin relaxation time when a weak magnetic field is applied. In the experimental range, the longest T_1 was found for a residual doping concentration as it has been observed in previous references for bulk direct-band-gap semiconductors: $T_1 \sim 10$ μs at the Zeeman splitting energy of 6.5 μeV. By comparing this value with values obtained for CdTe in Ref. [24], we conclude that a crossover point, as observed in high-purity bulk GaAs and InP, could also exist for CdTe. We have explained the fast increase of T_1 by the suppression of the two main zero-field mechanisms: hyperfine interaction and anisotropic exchange interaction related to the spin-orbit coupling. At higher magnetic fields, we have identified that the dominant mechanism is the electron hopping between donor impurities in samples

below the MIT transition. This successful application of the model proposed by Lyubinskiy to the experimental data in a CdTe QW opens interesting perspectives of applications to other II–VI and III–V materials.

In the context of the spin-based quantum information, the behavior showed by residual doped samples at low magnetic fields indicate they are an attractive candidate to obtain long spin relaxation times, which is one of the principal requirements for any qubit candidate.

In the whole insulating regime, the spin lifetime is driven by hyperfine interaction, anisotropic exchange, and hopping induced processes, the two latter being induced by the spin-orbit interaction. From our study on the full insulating range, one can deduce that lowering the doping, far from the MIT, will strongly reduce the efficiency of both spin-orbit related mechanism (by increasing the correlation and hopping times) at low and high field. The spin lifetime is then only limited by the hyperfine interaction. In the context of the spin-based quantum information applications one can then increase T_1 at low magnetic field by increasing the spin dephasing time T_Δ^e, which is limited by the interaction of the electron spin with the surrounding nuclear environment. This can be pursued by using isotopically purified materials. Isotopic purification is especially favorable in II–VI materials because they mostly have zero nuclear spins, while being commercially available.

ACKNOWLEDGMENT

We acknowledge F. Breton for the development of the data acquisition program.

[1] P. M. Koenraad and M. E. Flatté, Nat. Mater **10**, 91 (2011).
[2] G. Ethier-Majcher, P. St-Jean, G. Boso, A. Tosi, J. F. Klein, and S. Francoeur, Nat. Commun. **5**, 3980 (2014).
[3] K.-M. C. Fu, W. Yeo, S. Clark, C. Santori, C. Stanley, M. C. Holland, and Y. Yamamoto, Phys. Rev. B **74**, 121304(R) (2006).
[4] D. J. Sleiter, K. Sanaka, Y. M. Kim, K. Lischka, A. Pawlis, and Y. Yamamoto, Nano Lett. **13**, 116 (2013).
[5] A. Abragam, *The Principles of Nuclear Magnetism* (Oxford University Press, Oxford, 1961), p. 44.
[6] J. M. Kikkawa and D. D. Awschalom, Phys. Rev. Lett. **80**, 4313 (1998).
[7] R. I. Dzhioev, K. V. Kavokin, V. L. Korenev, M. V. Lazarev, B. Ya. Meltser, M. N. Stepanova, B. P. Zakharchenya, D. Gammon, and D. S. Katzer, Phys. Rev. B **66**, 245204 (2002).
[8] J. G. Lonnemann, E. P. Rugeramigabo, M. Ostereich, and J. Hübner, Phys. Rev. B **96**, 045201 (2017).
[9] I. Malajovich, J. M. Kikkawa, D. D. Awschalom, J. J. Berry, and N. Samarth, J. Appl. Phys. **87**, 5073 (2000).
[10] A. Greilich, A. Pawlis, F. Liu, O. A. Yugov, D. R. Yakovlev, K. Lischka, Y. Yamamoto, and M. Bayer, Phys. Rev. B **85**, 121303(R) (2012).
[11] D. Sprinzl, P. Horodyská, N. Tesařová, E. Rozkotová, E. Belas, R. Grill, P. Malý, and P. Němec, Phys. Rev. B **82**, 153201 (2010).
[12] G. Garcia-Arellano, F. Bernardot, G. Karczewski, C. Testelin, and M. Chamarro, Phys. Rev. B **99**, 235301 (2019).
[13] G. Garcia-Arellano, F. Bernardot, G. Karczewski, C. Testelin, and M. Chamarro, Phys. Rev. B **100**, 205305 (2019).
[14] S. Ghosh, V. Sih, W. H. Lau, D. D. Awschalom, S.-Y. Bae, S. Wang, S. Vaidya, and G. Chapline, Appl. Phys. Lett. **86**, 232507 (2005).
[15] B. Beschoten, E. Johnston-Halperin, D. K. Young, M. Poggio, J. E. Grimaldi, S. Keller, S. P. DenBaars, U. K. Mishra, E. L. Hu, and D. D. Awschalom, Phys. Rev. B **63**, 121202(R) (2001).
[16] J. H. Bus, J. Rudolph, S. Shvarkov, H. Hardtdegen, A. D. Wiek, and D. Hagele, Appl. Phys. Lett. **102**, 192102 (2013).
[17] D. Guzun, E. A. DeCuir Jr., V. P. Kunets, Y. I. Mazur, G. J. Salamo, S. Q. Murphy, P. A. R. Dilhani Jayathilaka, T. D. Mishima, and M. B. Santos, Appl. Phys. Lett. **95**, 241903 (2009).
[18] B. N. Murdin, K. Litvinenko, J. Allam, C. R. Pidgeon, M. Bird, K. Morrison, T. Zhang, S. K. Clowes, W. R. Branford, J. Harris, and L. F. Cohen, Phys. Rev. B **72**, 085346 (2005).
[19] I. A. Merkulov, AI. L. Efros, and M. Rosen, Phys. Rev. B **65**, 205309 (2002).
[20] P.-F. Braun, X. Marie, L. Lombez, B. Urbaszek, T. Amand, P. Renucci, V. K. Kalevich, K. V. Kavokin, O. Krebs, P. Voisin, and Y. Masumoto, Phys. Rev. Lett. **94**, 116601 (2005).
[21] K. V. Kavokin, Phys. Rev. B **64**, 075305 (2001).
[22] K. V. Kavokin, Phys. Rev. B **69**, 075302 (2004).
[23] J. S. Colton, M. E. Heeb, P. Schroeder, A. Stokes, L. R. Wienkes, and A. S. Bracker, Phys. Rev. B **75**, 205201 (2007).
[24] X. Linpeng, T. Karin, M. V. Durnev, R. Barbour, M. M. Glazov, E. Y. Shermaman, S. P. Watkins, S. Seto, and K.-C. Fu, Phys. Rev. B **94**, 125401 (2016).
[25] X. Linpeng, M. L. K. Viitaniemi, A. Vishnuradhan, Y. Kozuka, C. Johnson, M. Kawasaki, and K.-M. C. Fu, Phys. Rev. Appl. **10**, 064061 (2018).
[26] J. S. Colton, T. A. Kennedy, A. S. Bracker, and D. Gammon, Phys. Rev. B **69**, 121307(R) (2004).
[27] V. V. Belykh, E. Evers, D. R. Yakovlev, F. Fobbe, A. Greilich, and M. Bayer, Phys. Rev. B **94**, 241202(R) (2016).
[28] V. V. Belykh, K.V. Kavokin, D. R. Yakovlev, and M. Bayer, Phys. Rev. B **96**, 241201(R) (2017).
[29] M. Kroutvar, Y. Ducommun, D. Heiss, M. Bichler, D. Schuh, G. Abstreiter, and J. J. Finley, Nature (London) **432**, 81 (2004).
[30] J. Tribollet, E. Aubry, G. Karczewski, B. Sermage, F. Bernardot, C. Testelin, and M. Chamarro, Phys. Rev. B **75**, 205304 (2007).
[31] M. Chamarro, F. Bernardot, and C. Testelin, J. Phys: Condens. Matter **19**, 445007 (2007).
[32] K. De Greve, S. M. Clark, D. Sleiter, K. Sanaka, T. D. Ladd, M. Panfilova, A. Pawlis, K. Lischka, and Y. Yamamoto, Appl. Phys. Lett. **97**, 241913 (2010).
[33] C. Testelin, B. Eble, F. Bernardot, G. Karczewski, and M. Chamarro, Phys. Rev. B **77**, 235306 (2008).
[34] Y. M. Kim, D. Sleiter, K. Sanaka, D. Reuter, K. Lischka, Y. Yamamoto, and A. Pawlis, Curr. Appl. Phys. **14**, 1234 (2014).

[35] I. S. Lyubinskiy, JETP Lett. **88**, 814 (2008).
[36] A. A. Kiseleva, E. L. Ivchenkoa, A. A. Sirenko, T. Ruf, M. Cardona, D. R. Yakovlev, W. Ossauc, A. Waag, and G. Landwehr, J. Cryst. Growth **184**, 831 (1998).
[37] M. I. D'yakonov and V. I. Perel, Zh. Eksp. Teor. Fiz. **65**, 362 (1973) [Sov. Phys. JETP **38**, 177 (1974)].
[38] K. V. Kavokin, Semicond. Sci. Technol. **23**, 114009 (2008).
[39] A. V. Khaetskii and Y. V. Nazarov, Phys. Rev. B **64**, 125316 (2001).
[40] Yu. A. Bychkov and E. I. Rashba, Pis'ma Zh. Eksp. Teor. Fiz. **39**, 66 (1984) [JETP Lett. **39**, 78 (1984)].
[41] G. Dresselhaus, Phys. Rev. **100**, 580 (1955).
[42] Note that in Eqs. (15) and (17) of Ref. [35], an undefined coefficient $g(\vec{e}_0)$ appears. Using the definition of the spin precession frequency $\Delta\boldsymbol{\Omega}(\mathrm{t}) = \boldsymbol{\Omega}_0 \times \hat{\alpha}\, \boldsymbol{r}(t)/L_s$ when integrating Eq. (9), it is deduced that $g(\vec{e}_0) = \frac{1}{2}\,(\vec{e}_0 \times \hat{\alpha}\vec{e}_x)^2 + \frac{1}{2}\,(\vec{e}_0 \times \hat{\alpha}\vec{e}_y)^2$. When the Dresselhaus is the dominant spin-orbit coupling term, one obtains $g(\vec{e}_0) = 1$.